Self-Generated Magnetic Fields in the Microwave Plasma Resonant Interaction*

W. F. DiVergilio,† A. Y. Wong,† H. C. Kim, and Y. C. Lee†
TRW Systems, Redondo Beach, California 90278
(Received 8 November 1976)

The laser plasma interaction is simulated by the interaction of a microwave beam with an inhomogeneous, collisionless plasma. Magnetic fields are generated perpendicular to the density gradient and to the incident-wave polarization. The observed sharp reversal of field direction in the resonant region supports resonant absorption as the generation mechanism.

Self-generated dc magnetic fields have recently been observed both in laser plasma interactions[1,2] and in computer simulations.[3,4] Observations of the laser plasma have provided measurements of the magnitude of the field, but not the detailed geometry in the source region. Knowledge of the field geometry may lend important insight into which of the various proposed physical generation mechanisms[3-6] is dominant. We have studied the resonant interaction of an electromagnetic wave with a laboratory plasma amenable to detailed probe diagnostics.

The plasma is produced by a dc discharge at one end of a large (2-m-diam, 4-m-long) multidipole device, such that the plasma possesses a linear density gradient of typical scale length $L = 100-200$ cm $[n = n_c(1+z/L)]$. Typical operating parameters are the following: argon neutral pressure $(3-9)\times10^{-4}$ Torr, maximum density 4×10^{10} cm^{-3}, $T_e \simeq 1$ eV, and $T_i \simeq 0.1$ eV. Electrons are essentially collisionless, with $\nu^{ee} \simeq \nu^{ei} \simeq \nu^{en} \lesssim 10^{-3} f_{pe}$. A 20° horn at the low-density end of the chamber radiates an rf burst (maximum peak power 15 kW, pulse length 0.4–14 μsec at 1.2 GHz), which exhibits a strong resonant interaction with the plasma at the critical density layer ($n_c \simeq 1.8\times10^{10}$ cm^{-3}). One kilowatt of incident power corresponds to a maximum power density of approximately 3 kW/m^2, or $E_0^2/8\pi nkT_e \simeq 1.7\times10^{-3}$ at critical density, where E_0 is the electric field in the absence of the plasma. A detailed description of the device and some of the characteristics of the resonant interaction have been previously published.[7,8]

Magnetic field measurements were made by detecting the time derivative of the field with a 2-cm-diam, ten-turn center-tapped, electrostatically shielded magnetic loop probe. Pickup was found to be a major problem due to the large rf fields present. The center tap of the coil was grounded and the difference between the coil end outputs taken with a Tektronix 1A1 amplifier to eliminate further pickup. The magnetic probe was mounted on a movable probe shaft along with a Langmuir probe for density measurements. Three-dimensional probing of the interaction region was made possible by inserting the probe shaft into the system axially through a bellows and driving the shaft with a system of three coupled mechanical drives. The magnetic loop could be rotated to measure B_x and B_y, the field components perpendicular to the density gradient. A second magnetic loop entered the system radially for measurement of B_y and B_z.

A quasistatic magnetic field was observed to be generated in the resonance region by the incident electromagnetic wave. The magnetic field, B, is perpendicular to the density gradient and to the incident-wave polarization. Figure 1 illustrates the spatial dependence of B_y in the x-z plane ($y = 0$), where the density gradient is along z and the incident wave is polarized in the x direction. The traces in Fig. 1(a) were obtained by sampling the integrated probe output near the end of a 2.5-μsec microwave burst of peak power 7 kW.

For a given radial position x, B_y is seen as a function of z to peak near the critical density and to reverse sign 5–10 cm below critical, indicating the presence of a current layer in the resonant region flowing in the x direction. B_y also changes sign in the radial direction, with $B_y \simeq 0$ at $x = 0$. This geometry is explained by the following physical picture. The incident wave undergoes strong absorption in the resonant region. The x component of the absorbed wave momentum drives an electron current along the critical layer, while space-charge forces along the density gradient transfer the z component of momentum to the ions. Referring to Fig. 1(b), we note that the divergent incident wave drives a current in opposite directions on either side of $x = 0$, resulting in the observed radial sign change in B_y. The field geometry is essentially identical to that predicted by Thomson, Max, and Estabrook,[3] when their results are extended to a divergent source. The orthogonal relationship between the

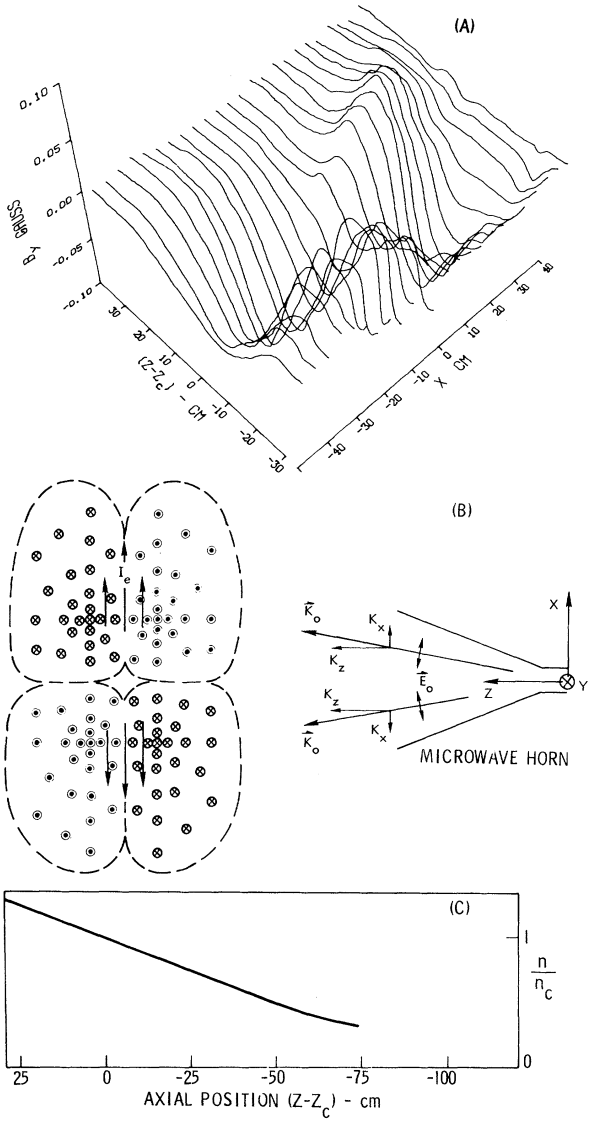

FIG. 1. (a) Steady-state B_y as a function of axial position, z, and radial position, x. Positive B_y corresponds to field in positive y direction, which points into the paper in (b). (b) Diagram of results shown in (a), indicating geometry of field with respect to microwave source. Inferred electron current paths are shown by solid lines and possible return paths by dotted lines. (c) Axial density gradient before rf turn-on. Position scale applies to (b) and (c).

quasistatic magnetic field and the incident-wave polarization was found to be preserved when the polarization was changed by rotating the microwave horn. In the remainder of the Letter, the polarization will be taken to be in the x direction.

Away from the plane $y = 0$, the functional form of $B_y(x, z)$ is unchanged, while the magnitude falls off as the microwave power density decreases. The maximum values of B_x and B_z were found to be always less than 0.2 of the maximum value of B_y. Some of these features are illustrated in Fig. 2, which shows B_x and B_y components in a plane of constant axial position, z. Probe orientation is the angle between the magnetic-loop axis and the y axis. Note that B_y changes sign as a function of x, as previously discussed, and falls off monotonically in the y direction away from $y = 0$. The smaller B_x signal may be due to a component of polarization in the y direction or to slight misalignment of the probe with respect to the horn.

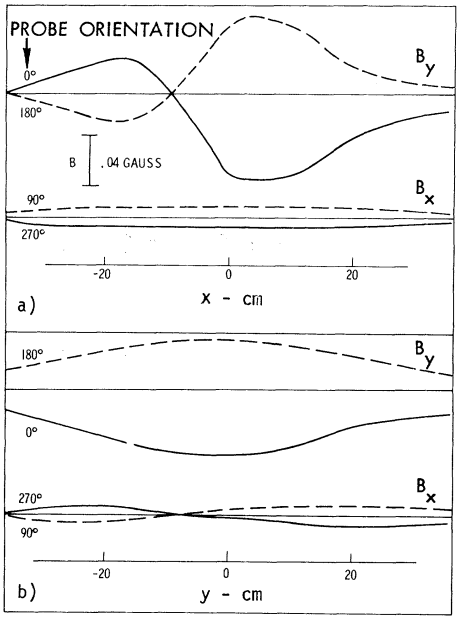

FIG. 2. Radial components of magnetic field at fixed axial position of maximum field, (a) as a function of x for $y = 10$ cm, (b) as a function of y for $x = 10$ cm. The fixed y and x positions for (a) and (b), respectively, were chosen to be far from lines of $B = 0$. Note the signal sign reversal for probe orientations differing by 180°, indicating the magnetic origin of the signal.

We have assumed up to this point that constant density surfaces lie in the x-y plane, and therefore, that the point of normal wave incidence is at $x = y = 0$. Note with reference to Fig. 2 that the radial sign reversal does not occur exactly at $y = 0$, but may be shifted as much as 10 to 15 cm off axis. This asymmetry was found to correlate well with a slight radial density gradient present in the plasma. Constant density surfaces are actually inclined at an angle, α ($0° < \alpha < 10°$), with respect to the x-y plane, moving the point of normal incidence to a position off the chamber axis. Radial density gradients should also have the ef-

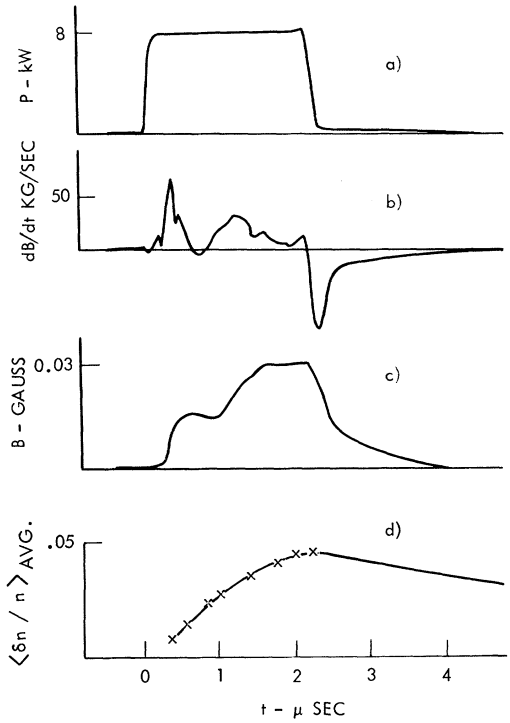

FIG. 3. Typical time dependence of magnetic field near critical layer. (a) Incident rf power as detected by a crystal detector. (b) Magnetic-loop probe signal, dB/dt. (c) Integrated probe signal, B. Long decay time of B is caused by long tail in rf pulse. (d) Spatially averaged density depletion, $L^{-1}\int_L(\delta n/n)dz$, near the critical layer, observed under similar plasma conditions as magnetic field data, but not concurrently. The resultant density profile becomes steeper.

fect of producing smaller components of magnetic field ($\sim B_y \sin\alpha$) in the x and z directions.

The magnetic field initially grows at the critical density and spreads to the underdense region. Typical time dependence of dB/dt and integrated B close to the critical layer is shown in Fig. 3. B rises to $B_{\max}/2$ in a time $\sim 500 f_{pe}^{-1}$ and saturates at $\sim 1800 f_{pe}^{-1}$. The steady-state field pattern illustrated in Figs. 1 and 2 is fully developed by $2000 f_{pe}^{-1}$. Langmuir probe measurements reveal that a density cavity is created at the resonant location by the expulsion of particles by the ponderomotive force. The density cavity develops in time into a plateau (typically 15 cm in extent in the z direction) in front of a sharp density step ($0.85 n_c$ to $1.1 n_c$ in 3 cm). The time development of the plateau is illustrated in Fig. 3(d) and is seen to correlate well with the establishment of the steady-state B field. Both the density step and steady-state magnetic field have been observed to persist for as long as $17\,000 f_{pe}^{-1}$, the maximum microwave pulse length available. We infer from concurrent density and magnetic field measurements that the field source is a current sheet flowing perpendicular to the density gradient at the position of the density step.

The source current is identified as the time-averaged current carried by the linearly converted electron plasma waves:

$$\langle \vec{J} \rangle = \langle n_1 e \vec{v}_1 \rangle = -\frac{e}{i4\pi m\omega}\frac{\omega^2}{\omega_p^2}\langle(\nabla\cdot\vec{E})\vec{E}\rangle, \qquad (1)$$

where Poisson's equation and the equation of motion have been used to obtain the right-hand expression. This expression points out that a rotation of the polarization field, $\vec{E}$, causes a rotation in the current, $\vec{J}$, and hence in the magnetic field. A wave polarized in the x-z plane generates electron plasma waves with electric field, and hence current components in the x and z directions. In the long-time limit, space-charge forces cancel the current component along the density gradient, leaving only the perpendicular component, $\langle J_x \rangle$.

An upper limit on the current density may be obtained by considering the flow of the x component of momentum from the incident wave to the electrostatic wave. In the steady state, momentum is carried into the resonant region at the speed of light and is carried out at some characteristic group velocity, v_g. The direction of momentum flow is in the direction of wave propagation, i.e., the z direction. We may write a momentum-flow balance equation

$$p_x^{es} v_g = a p_x^{em} c, \qquad (2)$$

where a is the absorption coefficient and p_x^{em} and p_x^{es} are, respectively, the x components of the electromagnetic and electrostatic wave momentum densities. p_x^{es} is obtained from the observed B field through Ampere's Law,

$$\frac{e}{m}p_x^{es} = -J_x = +\frac{c}{4\pi}\frac{\partial B_y}{\partial z}$$

$$\simeq 10^7 \text{ cgs esu } (\simeq 0.03 n_0 e v_{the}), \qquad (3)$$

at an incident power of 8 kW, or $E_0^2/8\pi nTe = 1.4 \times 10^{-2}$, and an incidence angle of 10°. The group velocity, v_g in Eq. (2), has been experimentally measured[9] by irradiating the plasma with two incident waves, ω_1 and ω_2, with frequency difference $\Delta\omega$, $\Delta\omega/\omega \simeq 10^{-4}$. The beat pattern between the two linearly converted plasma waves gives a

measurement of the group velocity $v_g = \Delta\omega/\Delta k \approx 10^6$ cm/sec in the vicinity of the resonant location. With p_x^{em} from the known incident power and horn radiation pattern, we obtain the reasonable value of 0.2 for the absorption coefficient, a.

The observed field geometry would appear to be inconsistent with a thermoelectric source. Since, at late times, ∇n is monotonic, the sign reversal of B as a function of axial position would require that ∇T reverse sign in one tenth the electron mean free path. Possible effects associated with the ambient magnetic field (measured as 0.4 G in the vertical direction) were ruled out by rotating the microwave horn to establish the independence of the self-generated fields from the ambient field.

We are grateful to Dr. D. Arnush for his discussions and support. The technical assistance of Mr. M. D. Plummer in construction of the three-dimensional probe system is acknowledged.

*Work supported by Lawrence Livermore Laboratory under Contract No. 7950105.

†Also University of California at Los Angeles, Los Angeles, Calif. 90024.

[1]J. A. Stamper, K. Papadopoulous, S. O. Dean, E. A. McClean, and J. M. Dawson, Phys. Rev. Lett. 26, 1012 (1972).

[2]J. A. Stamper and B. H. Ripin, Phys. Rev. Lett. 34, 138 (1975).

[3]J. J. Thomson, C. E. Max, and K. Estabrook, Phys. Rev. Lett. 35, 663 (1975).

[4]B. Bezzerides, D. F. DuBois, D. W. Forslund, and E. L. Lindman, Phys. Rev. Lett. 38, 495 (1977).

[5]D. A. Tidman and R. A. Shanny, Phys. Fluids 17, 1207 (1974).

[6]J. A. Stamper and D. A. Tidman, Phys. Fluids 16, 2024 (1973).

[7]R. L. Stenzel, A. Y. Wong, and H. C. Kim, Phys. Rev. Lett. 32, 654 (1975).

[8]A. Y. Wong and R. L. Stenzel, Phys. Rev. Lett. 34, 727 (1975).

[9]A. Y. Wong, University of California at Los Angeles Report No. 277, 1976 (unpublished).

Dependence of Laser-Driven Compression Efficiency on Wavelength

R. L. McCrory
University of Rochester, Rochester, New York 14627

and

R. L. Morse
University of Arizona, Tucson, Arizona 85721

(Received 14 June 1976)

Efficiency of ablative implosion of laser-heated pellets is estimated from numerical simulations based only on classical thermal conduction. An inverse dependence of overall nuclear-yield ratio on wavelength is indicated in the visible and near-infrared range.

Extensive numerical simulations indicate the possibility of achieving energy breakeven (or better) from laser-driven spherical implosion of pellets containing thermonuclear fusion fuel.[1] Implosion is driven by ablation of material from the surface of a pellet by the absorbed laser energy. This energy is transported by thermal conduction from the surface of critical density, ρ_c, where it is absorbed from the incident laser light, through ablated material to the surface of the compressed pellet core, or ablation surface. For visible or infrared wavelengths λ, ρ_c is much less than the density of the pellet core and occurs in the low-density blowoff. For the Nd laser for which λ is 1.06 μm, the critical electron density is $n_{ce} = 10^{21}$ cm^{-3}, and in the compressed core, which is at solid densities or higher, $n_e \gtrsim 10^{23}$ cm^{-3}. The efficiency of a given laser fusion implosion and burn event may be thought of approximately as a time-ordered product

$$\eta_{LF} = \eta_L \eta_c \eta_H \eta_B, \tag{1}$$

where η_L is the laser efficiency.

We take the view that the power which is effectively absorbed into the pellet from the incident laser light is that power which is transported from the immediate vicinity of the critical surface, after losses through only partial absorption and any subclassical thermal conduction, and into the higher-density ablated material where mass and heat flow are classical. The efficiency of processes near the critical surface which convert incident laser power into this effective absorbed power, P, is η_c. The efficiency with which classical mass and heat flow then convert the absorbed power, P, through the ablation process,